JOURNAL OF SYNCHROTRON RADIATION
ISSN 1600-5775

Received 21 November 2014
Accepted 17 February 2015

Edited by W. E. White, SLAC National Accelerator Laboratory, USA

Keywords: ultrafast dynamics; warm dense matter; four-wave mixing.

EIS: the scattering beamline at FERMI

Claudio Masciovecchio,[a]* Andrea Battistoni,[a,b] Erika Giangrisostomi,[a,b] Filippo Bencivenga,[a] Emiliano Principi,[a] Riccardo Mincigrucci,[a,c] Riccardo Cucini,[a] Alessandro Gessini,[a] Francesco D'Amico,[a] Roberto Borghes,[a] Milan Prica,[a] Valentina Chenda,[a] Martin Scarcia,[a] Giulio Gaio,[a] Gabor Kurdi,[a] Alexander Demidovich,[a] Miltcho B. Danailov,[a] Andrea Di Cicco,[d] Adriano Filipponi,[e] Roberto Gunnella,[d] Keisuke Hatada,[d] Nicola Mahne,[a] Lorenzo Raimondi,[a] Cristian Svetina,[a] Roberto Godnig,[a] Alessandro Abrami[a] and Marco Zangrando[a]

[a]Elettra – Sincrotrone Trieste SCpA, SS 14 km 163.5 in AREA Science Park, I-34012 Basovizza, Italy, [b]Dipartimento di Fisica, Università degli Studi di Trieste, I-34127 Trieste, Italy, [c]Dipartimento di Fisica e Geologia, Università degli Studi di Perugia, I-06123 Perugia, Italy, [d]Physics Division, School of Science and Technology, Università di Camerino, via Madonna delle Carceri 9, I-62032 Camerino (MC), Italy, and [e]Dipartimento di Scienze Fisiche e Chimiche, Università degli Studi dell'Aquila, I-67100 L'Aquila, Italy. *Correspondence e-mail: claudio.masciovecchio@elettra.eu

The Elastic and Inelastic Scattering (EIS) beamline at the free-electron laser FERMI is presented. It consists of two separate end-stations: EIS-TIMEX, dedicated to ultrafast time-resolved studies of matter under extreme and metastable conditions, and EIS-TIMER, dedicated to time-resolved spectroscopy of mesoscopic dynamics in condensed matter. The scientific objectives are discussed and the instrument layout illustrated, together with the results from first exemplifying experiments.

1. Introduction

The Elastic and Inelastic Scattering (EIS) project at FERMI (in Elettra, Trieste, Italy; Allaria *et al.*, 2012*a*) is aimed at the development of two experimental end-stations, served by distinct photon transport systems and designed to exploit the unique features of the FERMI free-electron laser (FEL) sources for innovative investigations on excited condensed matter.

The EIS-TIMEX end-station began user operations in 2013 and is focused on ultrafast time-resolved studies of matter under extreme and metastable conditions (Di Cicco *et al.*, 2011*a*,*b*). The two main concerns at the basis of the instrumental design are hence: (i) the maximization of the FEL photon flux at the sample, needed to photo-excite solid specimens into extreme thermodynamic conditions (Lee *et al.*, 2003), and (ii) the possibility to exploit a large array of pump–probe options, with sub-ps time resolution. In order to meet the former requirement, EIS-TIMEX features an essential photon transport system, able to minimize intensity losses from the source to the sample and provide a focal spot of few μm^2 with beam-shaping capabilities (Svetina *et al.*, 2011). FEL fluences as large as 10^2 J cm^{-2} can thus be achieved. Beams of such fluxes with energies in the EUV/soft X-ray range of operation for FERMI can induce efficient and homogeneous ultrafast excitations in solid samples.

Concerning the pump–probe capabilities, the photon transport system includes a split-and-delay stage for FEL-pump/FEL-probe applications (with a time window of about 30 ps and a time resolution better than 10 fs) (Allaria *et al.*, 2010; Corso *et al.*, 2012). Alternatively, the FERMI source can

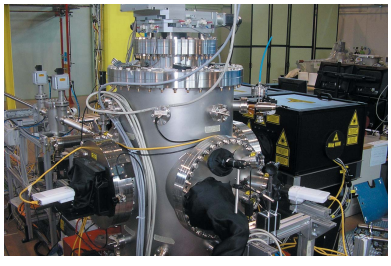

provide a two-color FEL emission with selectable separation between the two pulses, both in wavelength (within a variability interval of 2% for the seed) and in time (in the 0.2–1 ps range). The exploitation of both options allows for more complex sequences of FEL pulses at the sample. All this comes in addition to an IR–visible–UV setup for ultrafast pump–probe experiments which combines FEL and optical pulses. It is worth mentioning that such a setup holds the world-record timing jitter (∼6 fs) of any operating FEL (Danailov *et al.*, 2014).

The EIS-TIMER beamline will be dedicated to time-resolved spectroscopy of mesoscopic dynamics in condensed matter. At present the experimental end-station has been commissioned, while the complex photon transport system is under construction and is expected to be partially operational in 2015. The primary aim of EIS-TIMER is to exploit the full (*i.e.* both transverse and longitudinal) coherence of FERMI to extend coherent non-linear methods from the optical into the EUV/soft X-ray spectral domain. In this context, the main goal is to develop FEL-based four-wave-mixing (FWM) experiments (Tanaka & Mukamel, 2002; Bencivenga *et al.*, 2013; Guehr *et al.*, 2014), in particular those based on the transient grating approach. As these experiments rely upon the coherent interaction of three FEL pulses, the key requirement for the EIS-TIMER photon transport system is the capability to split the FEL beam into three parts, that have to be delayed and recombined at the sample at given angles. The idea for the basic configuration is to use both the first and third harmonics of the FEL emission: two first-harmonic pulses are sent to the sample with an interbeam angle 2θ in time coincidence, while a third-harmonic beam is time-delayed by a right-angle delay line, made out of four multilayer coated mirrors, and then impinges on the sample at an angle $\theta_B = \sin^{-1}(\sin\theta/3)$ to fulfill the so-called phase matching condition. The beam splitting is achieved by a sequence of two wavefront division beam splitters (Bencivenga & Masciovecchio, 2009; Cucini *et al.*, 2011*a*,*b*), while two additional plane mirrors steer the third harmonic beam into the delay line. The focusing of the beams at the desired angles is finally provided by three independent toroidal mirrors.

Such a configuration allows impulsive stimulated Brillouin, Raman and Rayleigh scattering experiments to be performed in the unexplored 0.1–1 nm^{-1} wavevector (Q) range, which is expected to be of the highest relevance for the study of dynamics in disordered systems and nanostructures (Bencivenga & Masciovecchio, 2009). The possibility offered by FERMI and EIS-TIMER to exploit the aforementioned two-color FEL emission, additional 'jitter-free' optical pulses and the independent control of the relative time delays between the three pulses (one of them limited to the −1 + 7 ps range), would allow further FWM-based experiments to be carried out, such as, for example, coherent Raman scattering (Tanaka & Mukamel, 2002; Boyd, 2010; Bencivenga *et al.*, 2014*a*) and photon echo or multi-dimensional spectroscopy (Mukamel, 1995). These methods are currently applied in the optical regime and have demonstrated their capability to probe a large array of dynamical processes, ranging from molecular vibrations to spin waves, with energy-wavevector selectivity and ultrafast time resolution, as well as to investigate dynamical processes inaccessible to linear light-matter interactions. The EUV/soft X-ray analogues of such techniques will potentially extend the range of investigable excitations towards high-energy modes, such as valence-band excitons, and will allow for nano to atomic spatial resolution, as well as for atomic selectivity, through the selective exploitation of core resonances (Tanaka & Mukamel, 2002; Bencivenga *et al.*, 2013, 2014*a*).

2. Scientific case and objectives

2.1. Matter under extreme conditions

Condensed matter exposed to high energy-density sub-ps pulses of light is rapidly driven into a nonequilibrium 'exotic' regime characterized by a hot electron subsystem and an unperturbed ionic subsystem. This condition relaxes in the ps time scale as the electrons and ions thermalize leading, under certain circumstances, to a warm dense matter (WDM) phase (Lee *et al.*, 2003). Both the exotic and the WDM regimes are almost unexplored experimentally and poorly described by available theoretical models. Experimental complexities reside in the extremely short lifetime that characterizes these phases as well as in the opacity of condensed matter to visible light. On the theoretical side, difficulties to model such transient states are ascribed to the poor control of microscopic mechanisms such as the electron–electron and electron–phonon coupling and their characteristic time scales under nonequilibrium extreme conditions of pressure and temperature. In addition, a comprehensive theoretical framework lacks, which is capable of satisfactorily describing a condensed material with solid densities and strong internal correlations but average temperatures in the realm of the plasma regime.

One of the principal aims of EIS-TIMEX is to investigate the electronic properties of both the exotic and the WDM regimes through spectroscopic techniques such as absorption and emission. The use of a laser/pump–FEL/probe approach with sub-10 fs time jitter, associated with a proper deconvolution procedure to clean out effects originated by long pulses, can guarantee the needed time resolution to monitor the collective electron dynamics after the pump absorption. A EUV FEL pump can be used to isochorically heat opaque specimens when laser pumps are not effective.

EIS-TIMEX is also aimed at elucidating the nature of intriguing phase transitions that lead to short living states of matter, such as the so-called low-density liquid (LDL) matter that is expected to show up when covalent systems lose their local open atomic order under the action of pressure and/or temperature. Such transient local structures in condensed matter are expected to be accessible by means of an ultrafast isochoric heating.

2.2. Coherent non-linear spectroscopy

When an electromagnetic field interacts with matter, the properties of the former can be modified. Optical spectro-

scopy is a longstanding and powerful branch of science devoted to the characterization of radiation–matter interactions and is widely used to study both the static and dynamic properties of matter.

In the second half of the 20th century the availability of synchrotron radiation sources has represented a revolution in this field, characterized by the advent of 'core-level' spectroscopies (as inelastic X-ray scattering, anomalous diffraction, X-ray absorption and emission, *etc.*). Such methods, still treated within the linear response theory, are able to add elemental and chemical sensitivity to the spectroscopic approach.

In parallel to the development of synchrotrons, another revolution in the field of optical spectroscopy was triggered by the invention of devices for light amplification by stimulated emission of radiation. Such LASER sources can be featured by high brightness, typically much more than synchrotron radiation, and, furthermore, by two other new and important characteristics, *i.e.* short time duration and coherence. The latter, in combination with the concept of pump–probe, allowed for time-resolved studies, able to monitor dynamical processes in real time. Nowadays, commercial lasers are able to deliver photon pulses with a time duration of a few tens of femtoseconds, while pulse durations as short as a single optical cycle [*i.e.* ∼2–4 fs in the visible–IR regime (Morgner, 2010; Goulielmakis *et al.*, 2008)] can be obtained using special setups. Laser-driven high-harmonic-generation processes can be used to generate attosecond pulses. Photon pulses of such a short duration paved the way to ultrafast (<ps) optical spectroscopy, that is currently used to study a large number of processes, such as: electronic dynamics (Li *et al.*, 1999), chemical reactions (Itatani *et al.*, 2004), molecular vibrations (Dhar *et al.*, 1994), charge transfer processes (Wynne *et al.*, 1994), *etc*. Coherence means that the electric field of the source at different places and times have fixed phase relationships, *i.e.* all photons in a laser pulse are (almost) in a 'single mode'. This special feature of laser radiation allowed several applications, such as those based, for example, of the concepts of interferometry and holography. Furthermore, coherence is an essential requisite to observe coherent non-linear processes even when the amplitude of the fields is substantially lower than the atomic/molecular field.

In a non-linear experiment the interaction between the incoming electric fields (E) and the sample can be accounted by a power series expansion in E of the induced polarization:

$$P = \varepsilon_0\left[\chi^{(1)}E + \chi^{(2)}EE + \chi^{(3)}EEE + \ldots\right] \qquad (1)$$

where $\chi^{(n)}$ are $n+1$ rank tensors known as nth-order susceptibility. In general, the even-order terms of χ are null in any centro-symmetric system (Boyd, 2010). Therefore, the lowest-order non-linear processes for all samples are the third-order ones, that are at the basis of FWM applications. FWM experiments are hence based on the interaction of three photon pulses with the sample, resulting in a (fourth) coherently scattered beam containing the information on the system under study. Since the photon frequency, wavevector, bandwidth, polarization and arrival time of the three incoming pulses can be different from each other, different kinds of FWM experiments can be performed and used to probe various dynamical processes, arising from different components of the χ tensor. Among such classes of experiments, we can cite the optical Kerr effect, spin-photon echo spectroscopy, coherent antistokes Raman scattering, multi-dimensional spectroscopy (Cundiff & Mukamel, 2013), stimulated Rayleigh and Brillouin scattering (Dhar *et al.*, 1994), *etc*. In general, the only condition that has to be met in all these experiments is the 'phase matching', which essentially accounts for energy–momentum conservation in the non-linear process. Indeed, the strength of the FWM field can usually be cast in the form (Boyd, 2010; Bencivenga *et al.*, 2013)

$$E_4(\underline{k}_4, \omega_4) \propto \chi^{(3)} E_1(\underline{k}_1, \omega_1)\, E_2(\underline{k}_2, \omega_2)\, E_3(\underline{k}_3, \omega_3)\, \mathrm{sinc}\left(\frac{\Delta\underline{k}\,\underline{L}}{2}\right) \qquad (2)$$

where $\omega_4 = \sum_{i=1}^{3} \pm\omega_i$ and $\underline{k}_4 = \sum_{i=1}^{3} \pm\underline{k}_i$ are a given combination of the input photon frequencies and wavevectors, while $\Delta\underline{k} = \underline{k}_4 - \sum_{i=1}^{3} \pm\underline{k}_i$, and $\underline{L}$ is the optical path length. The 'sinc' term accounts for the phase matching and has a twofold consequence: on one hand an appreciable non-linear signal can be detected only when $\Delta\underline{k} = 0$, and, on the other hand, such signal is localized in a well defined direction of space. The latter fact can be exploited to '*a priori*' select the direction of the FWM signal, which can be often chosen different from those of the input beams. The possibility to look for a time-dependent 'showing up' of the FWM signal over the background usually results in a large enhancement in the signal/noise ratio with respect to other pump–probe methods, in which time-dependent variations of some signals (reflectivity, transmission, *etc*.) have to be detected.

The next relevant step forward for optical spectroscopy would be to combine core-level spectroscopies and their elemental selectivity with time-resolved methods and non-linear techniques (Adams, 2011). To do so, we need novel photon sources capable of delivering ultrafast EUV/X-ray photon pulses with coherence properties comparable with those of table-top lasers. Toward this direction is moving the development of HHG (high harmonics generation) sources (Gallmann *et al.*, 2012) that, at the present stage, however, are not brilliant enough for FWM applications.

A new era has begun with the advent of EUV/X-ray FELs (Emma *et al.*, 2010). These are much brighter than HHG sources and are able to provide radiation which is (almost) as coherent as optical lasers spatially, and, in the case of seeded sources like FERMI, also temporally (Allaria *et al.*, 2012*a*). Thanks to the advances achieved during the last few years, which also include the development of multi-color FEL sources (Lutman *et al.*, 2013; Allaria *et al.*, 2013; Hara *et al.*, 2013; Bencivenga *et al.*, 2013; Guehr *et al.*, 2014), non-linear coherent experiments in the EUV/X-ray regime are no longer a mere theoretical speculation. These experiments would allow the study of, for example, ultrafast charge migrations

and energy transfer processes with nanometric to atomic spatial resolution and elemental selectivity (Tanaka & Mukamel, 2002; Bencivenga *et al.*, 2013), as well as of collective atomic dynamics in the unexplored (0.1–1 nm^{-1}) wavevector range, which is of the highest relevance for disordered systems and nanostructures (Bencivenga & Masciovecchio, 2009; Cucini *et al.*, 2011*a*).

2.3. Transient grating experiments

The first simple step towards the direction of (non-degenerate) EUV/X-ray FWM applications is to consider the particular case in which two pulses having the same polarization and photon frequency are crossed into a sample in time coincidence, and the elastically scattered third pulse is observed. This scheme, also known as transient grating (TG), allows, for example, impulsive stimulated Rayleigh, Brillouin and Raman scattering processes (Dhar *et al.*, 1994), that are at the basis of the rationale of the EIS-TIMER project, to be exploited. In a generic TG experiment (see Fig. 1) the interference of the two time-coincident pulses results in a standing electromagnetic wave with spatial periodicity $\Lambda = \lambda/2\sin\theta$, where λ and 2θ are the wavelength and crossing angle of the two interfering pulses, respectively. Such an excitation couples with the internal degrees of freedom of the sample, leading to a modification of the optical properties of the material. The time evolution of the induced grating encodes the time evolution of the sample's excitations with wavevector (Q) equal to that of the grating ($2\pi/\Lambda$). These effectively couple with the induced transient grating and their time evolution can be probed by looking at the diffraction of a third (time delayed) pulse, provided that the latter fulfills the phase matching conditions, which, in such TG experiments, reduces to the Bragg scattering condition. In the first few femtoseconds the interactions only involve the electronic degrees of freedom, while at picosecond time scales rearrangements of atomic density fluctuations, such as inter- and intra-molecular vibrations, occur. Slower processes like, for example, heat and particle diffusions take place at much longer times (>ns).

One of the main aims of TIMER is to study the time evolution of density fluctuations in disordered systems (liquids and glasses), in the unexplored ('mesoscopic') wavevector (Q) range between 0.1 nm^{-1} and 1 nm^{-1} (Bencivenga & Masciovecchio, 2009; Cucini *et al.*, 2011*a*). The study of density fluctuations, particularly the Q-evolution of acoustic modes, in disordered systems is a very active field of research. From such kind of study one can gain information about the microscopic processes that are responsible for the macroscopic mechanical and thermodynamical properties of the material. In particular, some of the most debated topics concern: (i) the understanding of the liquid–glass transition, (ii) the excess low-temperature specific heat and the excess density of vibrational states in glasses, (iii) the microscopic origin of sound attenuation in glasses and viscosity in liquids, *etc*.

Key characteristics of disordered systems are the lack of spatial periodicity and the presence of additional degrees of freedom with respect to the crystalline phase, like, for example, diffusion and relaxation processes in liquids as well as hopping and tunneling processes in glasses. In order to thoroughly characterize the processes arising in disordered systems it is not sufficient to limit the study to a given Q-region (as Brillouin zones for the case of crystals), but it is necessary to exploit a range in Q and ω (here $\omega = c_s Q$ is the acoustic frequency, where c_s is the sound velocity) as large as the inverse characteristic length and time scales of the dynamical processes of interest. This consideration is among the reasons that pushed the impressive development of different techniques able to follow the acoustic modes evolution from femtosecond to microsecond time scales and from micrometer to picometer length scales. Fig. 2 represents the time–space/ω–Q plane, in which we report an overview of most of the currently available techniques to probe the dynamics of density fluctuations; full and dotted inclined red lines represent some typical $\omega(Q)$ dispersions in condensed matter.

Optical TG and ultrasonic methods (not shown in Fig. 2) are able to probe the low-Q region of the ω–Q plane, essentially irrespectively to the time scale range, while, also thanks to some recently developed tools and instrumentation (Bencivenga *et al.*, 2012; Battistoni *et al.*, 2014; Masciovecchio *et al.*,

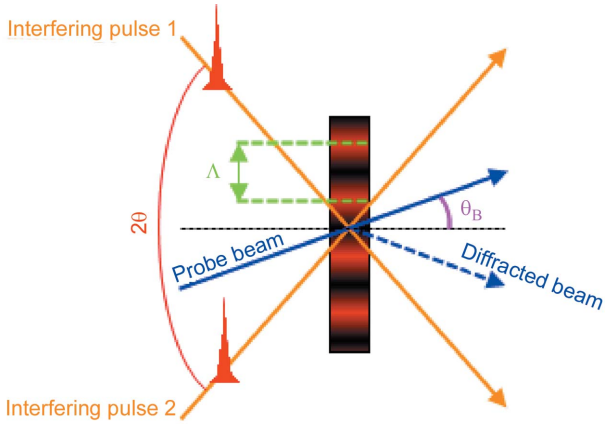

Figure 1
Typical scheme of a transient grating experiment.

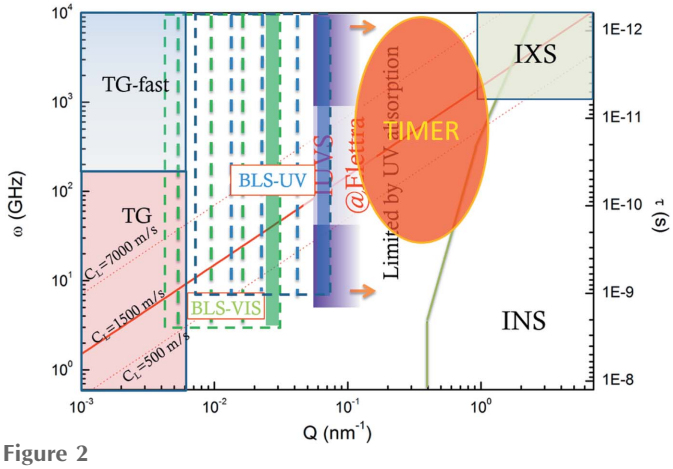

Figure 2
From lower to higher Q-values the reported techniques are: optical TG, Brillouin light and UV scattering (BLS-VIS, BLS-UV and IUVS) and inelastic X-rays and neutrons scattering (IXS, INS).

2004), one can use frequency-resolved Brillouin scattering to cover with continuity the visible–UV spectral range. The high-Q range of the ω–Q plane is the realm of atomic-size probes, such as hard X-rays and thermal neutrons, which can be inelastically scattered by high-Q atomic density fluctuations (Burkel, 2000; Lovesey, 1986). Between these low-Q and high-Q extrema, where matter looks like a continuum and an ensemble of distinct atoms, respectively, there is a no man's land, also referred to as 'mesoscopic' region, that extends from 0.1 nm^{-1} to 1 nm^{-1}. While the low-Q region can be described within classical elastic theory or hydrodynamics and the high-Q one can be modeled within the single-particle (incoherent) approximation, there are no well assessed models to describe the Q region between 0.1 and 1 nm^{-1} in systems without translational periodicity. Within such range, one would be able to directly observe the system transition between a hydrodynamic behavior (fully relaxed regime) and the single particle limit (not relaxed regime). The chance to have access to this spectral region will give us the unique opportunity to better understand the nature of the two physical limits and to shed light on the macroscopic anomalies of glasses, that are supposed to be found there. Thanks to the short-wavelength coherent radiation of the FERMI FEL, EIS-TIMER will be able to extend the TG approach to EUV/soft X-ray wavelengths in order to fully probe the mesoscopic region, hence unravelling the behavior of disordered systems in such a "no-man's land".

3. Layout of the instruments

3.1. The EIS-TIMEX end-station

The FEL is delivered to the experimental hall of FERMI through the photon analysis delivery and reduction system (PADRES) (Zangrando *et al.*, 2009), a section that, while transporting the photon beam to the various end-stations, hosts various tools for its manipulation and diagnostics: beam-defining apertures, beam position monitors, intensity monitors, gas absorbers, an energy spectrometer and a split and delay-line. As sketched in Fig. 3, a switching mirror before the split and delay-line directs the light to the EIS-TIMER end-station, whereas in a three-way switching chamber the light is diverted to either the EIS-TIMEX, the DiProI or the LDM end-station. Each end-station is served by its own focusing optics.

For EIS-TIMEX, a plane mirror (located in the three-way switching chamber) deviates the FEL towards an ellipsoidal

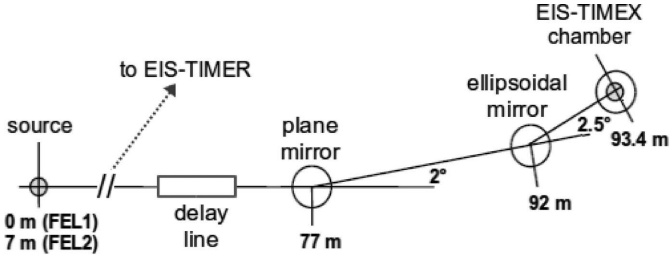

Figure 3
Sketch of the EIS-TIMEX beamline.

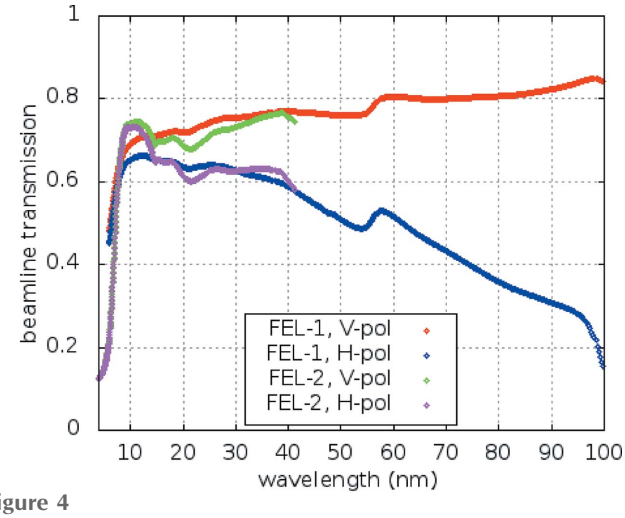

Figure 4
Beamline transmission including the final ellipsoidal mirror.

mirror, at a distance 15 m apart, that focuses the radiation 1.4 m downstream of it, at the center of a high-vacuum chamber hosting the sample and various diagnostics. As shown in Fig. 4, the overall beam transport transmittance is of the order of 65–70% for circularly polarized radiation in a wide wavelength range, substantially smaller only below 7 nm and above 70 nm. The vertical polarization always has a considerably higher transport efficiency than the horizontal one, with the larger differences occurring at lower energies.

The focal spot has a Gaussian shape with an estimated size of about 4.4 µm FWHM for FEL-1 and of about 2.3 µm FWHM for FEL-2. In the future, the plane mirror will be replaced by an active optics equipped with piezoelectric actuators that will allow the mirror profile to be altered thus obtaining the desired beam shape at focus (Svetina *et al.*, 2012). The main purpose is to gain control over the spatial distribution of the energy density deposited onto the sample; however, applications can be various. Non-negligible beam tails would, for example, make possible a direct measurement of the sample temperature raising with an infrared pyrometer, following the lines described by Principi *et al.* (2012).

Recently, an additional plane mirror has been accommodated in the same chamber that hosts the ellipsoidal mirror to offer the possibility of a fast switch between the described focusing setup and an alternative one featuring a focusing mirror placed inside the main EIS-TIMEX chamber (or even externally, in case users wish to bring their own chamber and place it downstream of EIS-TIMEX). For the last configuration, several spherical mirrors are at disposal, with a focal length of 200 mm and either a single or multilayer coating. Inevitably, the flux throughput will be reduced, due to a combination of lower reflectivity and larger spot size.

The main EIS-TIMEX chamber is illustrated in Fig. 5. It has a cylindrical shape with 500 mm internal diameter and is equipped with a five-axis manipulator that holds samples and fundamental beam imaging diagnostics like YAG, phosphor and diamond screens. Typical samples used for absorption measurements are thin self-standing foils (thickness 50–100 nm) provided by Luxel or Lebow, whereas samples for

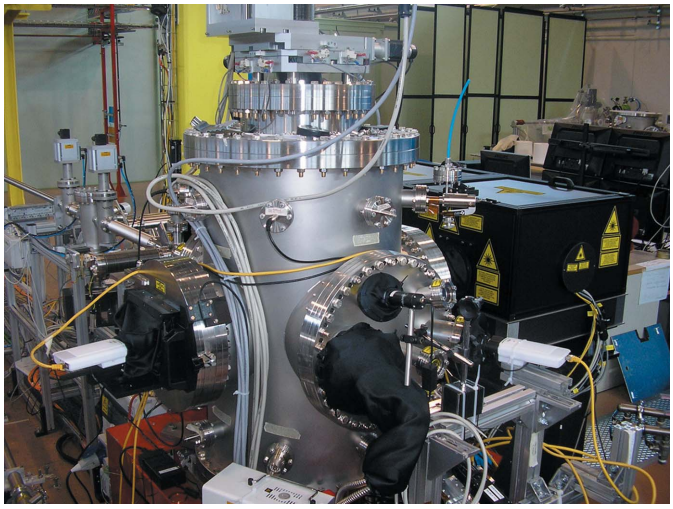

Figure 5
External view of the main EIS-TIMEX chamber. On the right one can distinguish the black box that protects the laser setup.

emission or reflectivity measurements are often thin depositions on proper substrates (*e.g.* Si) as well as single-crystal slabs. Rapid and precise positioning of the sample/screen under the beam is obtained by motorized movements along the optical axis, the horizontal axis, the vertical axis, the polar angle and the azimuthal angle.

The chamber is kept at a vacuum level of 10^{-8} mbar by a rotary pump coupled with a turbomolecular pump. Two GigaEthernet cameras from Axis Communications provide a wide view on the chamber inside, whereas close visual inspection of the sample/radiation interaction region is provided by a long-distance microscope from Questar placed at 35 cm from the chamber center at an angle of about 20° with respect to the direction of the incoming light. The telemicroscope exhibits a resolution better than 5 µm, a focal depth of a few tens of micrometers and a field of view of about 600 µm. It serves a number of purposes: to determine the beam focal plane and estimate *in situ* the spot size at the focus as well as to spatially superimpose the FEL beam on the laser (and both on the sample); to monitor the sample damage level upon more or less prolonged radiation exposure; and to provide feedback for focal plane adjustment to the algorithm that manages the sample movement in a serpentine path, based on the visualized damage craters. A 'locked' mode can be enabled in which the telemicroscope, with a combination of three motorized movements of the five-axis manipulator, rigidly follows the sample as this is translated along the FEL propagation axis, thus making easy an evaluation of the FEL caustic curve. When operated in an 'unlocked' mode, the telemicroscope remains stationary, thus offering a valid reference to position samples of different thicknesses at the same focal plane by moving the manipulator.

The beamline disposes of a set of photon detectors to be placed in transmission and reflection geometries. Mostly used are Si p-n junction photodiodes from IRD Inc. Both the AXUV and SXUV models fully cover the spectral range of interest. One or the other is chosen depending on the expected flux level at the detector, the first one featuring a higher sensitivity and the second one, on the contrary, a higher radiation hardness. Their wide dynamic ranges can be further extended by use of an amplifier (in cases of low irradiances), or by application of a reverse bias (in cases of high irradiances). Bolometers from Fortech HTS GmbH are also available, which have a more linear response in their µJ to mJ operational range but a significantly lower signal/noise ratio. According to our verifications, the short duration of the FEL pulses and/or their high intensity are such to render unreliable absolute pulse energy determination using supplied data sheets for the energy-dependent quantum efficiency. For this reason, we usually rely on a cross-calibration of these detectors with the ionization monitor available along the FEL transport system.

Custom detectors have been developed as well. These comprise detectors obtained by coupling Al-coated YAG fluorescence screens to photodiodes with enhanced sensitivity in the visible or to CCD cameras from Basler, solutions that present advantages in terms of non-linearity and damage risks. Further, as an in-chamber monitor of the incident intensity, it is possible to record the drain current associated with photoemission from the surface of the focusing mirror. The signals from these detectors are read out by either a four-channel picoampmeter (model AH401B, by Elettra-Sincrotrone Trieste) for low-current measurements (from 50 pA with a resolution of 50 aA up to 1.8 µA with a resolution of 1.8 pA) or by an eight-channel digitizer (model V1720, by CAEN) characterized by a 12-bit resolution and a 250 MS s^{-1} sampling rate.

On request, an EUV spectrometer can be made available, to be positioned either on the FEL axis or in reflectance/fluorescence geometries. Realised in the framework of an In-Kind Project for the EuroFEL consortium lead by CNR-IFN Padova and conceived with a compact and flexible design for portability at various end-stations (Frassetto *et al.*, 2014), it allows the wide energy range from 25 to 800 eV to be covered with high spectral resolution (better than 0.2% in the whole interval) and large acceptance angles (10 mrad × 17 mrad in the interval from 30 to 250 eV and 5 mrad × 17 mrad at 250–800 eV).

Since July 2013, with the completion of the user laser transport to the experimental hall, the EIS-TIMEX beamline has been equipped with an optical setup for combined laser/FEL pump–probe experiments. The laser available at EIS-TIMEX is a fraction of the seed laser pulse transported up to the end-station in a dedicated low-vacuum tube. With this approach the beamline can benefit from the natural synchronization between the FEL and laser pulses and provides low-jitter measurements (Cinquegrana *et al.*, 2014; Danailov *et al.*, 2014). The user laser comes up with typical pulse durations of 100–120 fs, and intensities up to 500 µJ. Within our setup, we can manage the attenuation level, the polarization status, as well as select between the fundamental radiation at 780 nm and its second (390 nm) and third (260 nm) harmonic. In the last two cases, the available intensity will be, by necessity, smaller and the pulse length may be slightly altered, despite

the use of compensator crystals. A motorized delay line allows the time delay to be adjusted relative to the FEL within an interval of ∼1.3 ns. Translation of a focusing optics permits to obtain a laser spot size variable between 30 and 200 µm FWHM. Fluorescence YAG screens have been found to overestimate the spot size of the FEL and to suffer the diffused back-reflected light when used with visible lasers. To estimate the laser footprint at the sample position, we therefore rely on 'a virtual sample' CCD camera that images a small fraction of the laser beam having passed through an identical path, thus also providing the signal for a feedback loop which acts on the high-precision piezo-driven tip-tilt mounts of the laser focusing mirror. Such a fine steering of the laser beam trajectory reflects in much improved pointing and timing stabilities, with great benefit for experiments that require high spatio-temporal superposition with the FEL beam (Danailov *et al.*, 2014). Another CCD camera collects the nearly back-reflected laser light in those pump–probe experiments where the laser acts as a probe. For experiments with a laser pump and a FEL probe, we are planning to substitute the present focusing optics with another one of shorter focal length, to be directly positioned inside the EIS-TIMEX chamber in order to reach higher laser fluences at the sample.

Figs. 6 and 7 illustrate in more detail the current configurations of, respectively, the external (*i.e.* in air) and internal (*i.e.* in vacuum) optical breadboards.

All hardware and software assets at FERMI are managed with the TANGO controls framework (http://www.tango-controls.org/). Each instrument is interfaced with a configurable TANGO device. During data acquisition (Borghes *et al.*, 2013), each device buffers its data tagged with the corresponding FEL pulse identification number. A higher level TANGO device, FERMIDAQ, collects the tagged data from the instruments and writes it to the storage system. Experimental data and metadata are organized and saved in a binary scientific data format, HDF5 (Hierarchical Data Format, http://www.hdfgroup.org/HDF5/). The acquisition system is highly configurable, allowing users to select from an all-comprehensive list which data sources should be stored. This list includes devices from both the end-station instrumentation and the machine diagnostic system. Collected datasets may be accessed securely through the Elettra's Virtual User Office (VUO). Various experimental sequences are coded as Python scripts and executed by a highly dynamic and flexible script engine, named EXECUTER. The graphical interface consists of configurable QTango applications, based on the QT framework.

Despite being in its early years of operation, the beamline is in an advanced status of automation and can be operated both at the maximum repetition rate of FERMI (nowadays 10 Hz) and in single-shot mode. For the last case, various algorithms have been developed to compensate for possible non-orthogonal positioning of the sample with respect to the incoming FEL beam, thus assuring controlled irradiation conditions. Since sample movement from one position to an adjacent one in the single-shot mode requires more than 1 s, the light beams have to be shuttered in between one pulse and the other, an operation that is accomplished by a fast shutter in the optical laser case and, for the FEL case, by desynchronizing the electron bunch and the seed laser beam. Procedures exist to launch delay line scans in either continuous or stepped modes with both the delay line of EIS-TIMEX, on the optical laser path, and that of the FERMI transport line, on the FEL path. Enabling the pump–probe option, maximum flexibility is left in the choice of the number of FEL and laser pulses before and after a time-zero pump–probe event. Therefore one may, for example, choose to probe the sample with the desired accuracy both before and after a given number of pump shots (whichever are the pump and the probe among the FEL and the optical laser). Although FERMI, as a seeded FEL facility, offers greater stability than other SASE FEL facilities, nonetheless each FEL pulse may differ in terms of energy, spectral content, spatial profile and/or beam pointing. For example, the pulse intensity may display fluctuations of the order of 10%, or even greater when the optical parametric amplifier (OPA) is used to tune the seed wavelength. Therefore, experimental data are treated on a statistical basis, sorted and filtered, if needed, according to the parameters of interest,

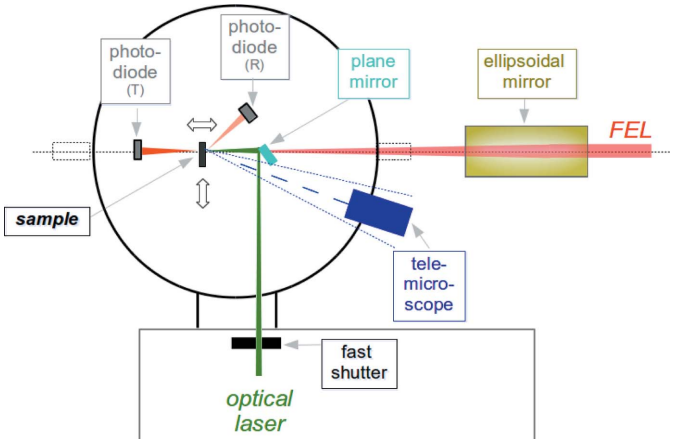

Figure 6
Sketch of the EIS-TIMEX main experimental setup based on an Au-coated ellipsoidal focusing optics (f = 140 cm).

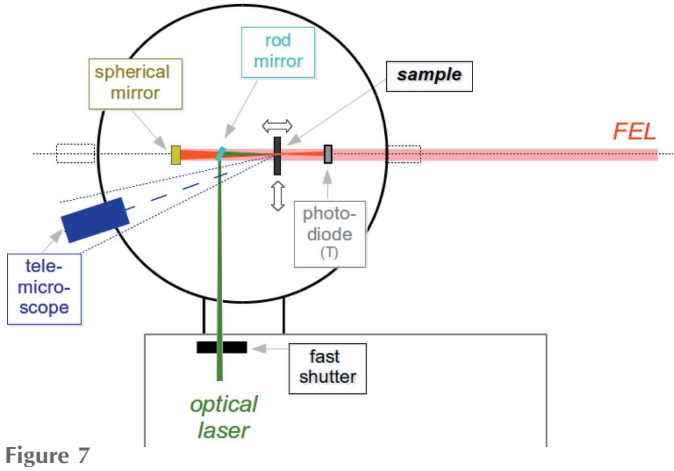

Figure 7
Sketch of an alternative setup based on a multilayer focusing optics with shorter focal length (f = 20 cm).

including those from the PADRES diagnostics and from upstream instrumentation in the accelerator and undulator sections of FERMI.

4. Layout of the EIS-TIMER end-station

The main issue to be taken into account in the design of the EIS-TIMER photon transport system is the high absorbance of all materials at the EUV/soft X-ray wavelengths of interest. This prevents the use of transmitting optics, such as phase masks (Maznev *et al.*, 1998), that are widely employed in traditional TG setups since they lead to a relevant simplification of the layout. The feasibility of an optical scheme based on all-reflecting optics and, in particular, on plane mirrors used as wavefront division beamsplitters was demonstrated in our laboratories by Cucini *et al.* (2011*b*). Such a strategy to obtain the three input pulses has also the advantage of avoiding any relevant pulse chirping.

The absence of phase masks makes it difficult to obtain a so-called local field, which can be used for heterodyne detection (HD) of FWM signals (Maznev *et al.*, 1998). HD is usually employed to largely enhance the overall signal, hence improving the signal/noise ratio, as well as to determine both amplitude and phase of the signal field. The latter capability can be profitably exploited to study particular kinds of excitations, as polaritons or spin waves. Actually, we recently demonstrated the possibility to use optical TG with homodyne detection to disentangle the dynamics related to rotational, orientational and translational degrees of freedom in liquids, a task usually achieved by HD-TG (Cucini *et al.*, 2014). In order to discriminate all these contributions, it was necessary to perform homodyne detected TG measurements varying the polarizations of the input beams, a solution which is also exploitable at EIS-TIMER thanks to the polarization tunability of the FERMI FEL.

Another issue to be discussed is related to the efficiency of FWM processes in the EUV/soft X-rays range. So far, only calculations and simulations have been performed to estimate EUV/X-ray FWM signals (Tanaka & Mukamel, 2002; Patterson, 2010; Bencivenga *et al.*, 2013, 2014*a*) while no experimental data at sub-optical wavelengths are available. In July 2014 we carried out the very first FWM experiment stimulated by EUV transient gratings (Bencivenga *et al.*, 2014*a*). We observed a detectable EUV-FWM signal from a vitreous SiO_2 sample, that allowed us to estimate an overall efficiency of the FWM process of about 1.5×10^{-7}, which, in light of our specific experimental conditions, is quite similar to that found in the optical regime. Other pioneering coherent non-linear X-ray experiments based on second-order processes (Glover *et al.*, 2012; Tamasaku *et al.*, 2011; Shwartz *et al.*, 2014) report a substantial reduction in the experimental signals with respect to the optical analogues. This could be either due to the shorter wavelengths of X-rays with respect to EUV photons or to the lower degree of longitudinal coherence of the employed photon sources, as compared with the almost Fourier transform limited pulses delivered by FERMI.

Fig. 8 sketches the conceptual layout of the EIS-TIMER beamline. To fully cover the mesoscopic region (Q = 0.1–1 nm^{-1}) it is necessary to exploit the whole wavelength range (100–10 nm) provided by FERMI and exploit large crossing angles (*i.e.* up to above 90°). We also mention that, following some reconsiderations of the FEL performance and machine upgrades, the minimum exploitable wavelength range of FERMI is now pushed down to the 3–4 nm range. As already stressed, in order to reduce the absorption losses of EUV radiation and to avoid chirping, the beamline was conceived to operate with reflection optics only (plane and focusing mirrors). A first plane mirror is used as a wavefront division beamsplitter in the vertical plane to split the beam into two halves. One of them is further split by another wavefront division plane mirror working in the horizontal plane into two halves that are used to excite the transient grating. The other half, deflected into a right-angle delay line by the other two plane mirrors (not shown in Fig. 8), is used to probe the induced grating. The delay line is equipped with four multilayer (ML) mirrors operating at 45° angle of incidence and optimized to reflect the third harmonic of the FEL radiation (wavelength λ_3), whose intensity is of about 1% of that of the first harmonic (wavelength λ_1); four sets of four MLs optimized for the 18, 13.3, 6.72 and 3.17 nm radiation will be available. Such MLs can provide an extinction ratio of the first over the third harmonic by more than six orders of magnitude, while the 45° geometry allows probing time delays as large as a few nanoseconds. Solid state filters can eventually be used to suppress the residual first harmonic component from the probe beam and/or the third harmonic content from the pump beams. In order to accomplish the phase matching conditions, the angles of incidence of the three beams at the sample have to satisfy the relation $\sin\theta/\lambda_1 = \sin\theta_B/\lambda_3$, where 2θ is the crossing angle between the two interfering first-harmonic beams and θ_B is the angle between the bisector of these beams and the probing third-harmonic beam. The three FEL pulses are finally focused onto the sample at the correct angles by a set of three toroidal mirrors (TMs). In order to change θ (and

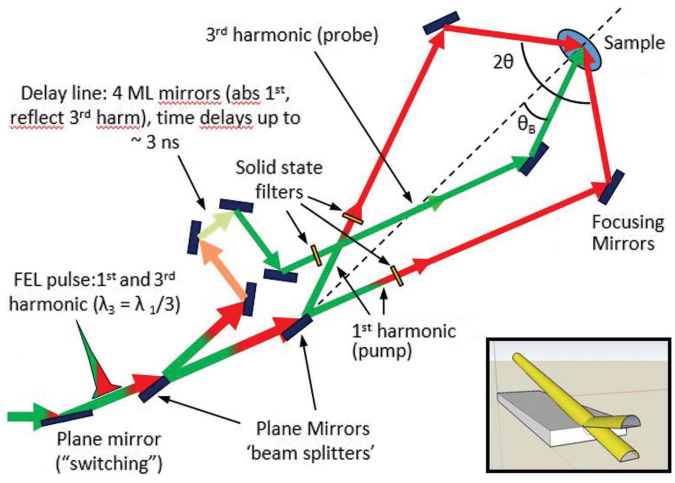

Figure 8
Sketch of the EIS-TIMER layout.

Table 1
Q-values available at EIS-TIMER (in nm^{-1}) as a function of θ (rows) and λ_1 (columns); the last two columns on the right correspond to λ_1 values achievable by FERMI but not foreseen by the present layout of EIS-TIMER.

	λ_1					
θ	54 nm	39.9 nm	20.16 nm	9.51 nm	5 nm	3 nm
9.2°	0.037	0.05	0.1	0.21	0.4	0.67
13.8°	0.055	0.075	0.15	0.32	0.6	1
39.5°	0.15	0.2	0.4	0.84	1.6	2
52.7°	0.19	0.25	0.5	1.05	2	3.3

θ_B accordingly) the three TMs can be removed from the beam path and three other TMs can be inserted downstream; four sets of three TMs will be available to exploit the angles θ = 9.2°, 13.8°, 39.5° and 52.7°. Since $\lambda_1 = 3\lambda_3$, a given set of MLs and TMs defines the actual Q-value, according to the relation $Q = 4\pi/\lambda_1 \sin\theta$ (see Table 1). In case one would exploit the full wavelength tunability of FERMI, an ultrafast ['jitter-free' (Danailov *et al.*, 2014)] optical pulse tunable in the VIS–UV range can be used as an alternative probe, though the longer wavelength of such a pulse will not allow the phase matching to be fulfilled in the entire λ range. We finally mention that the relative time delay between the two interfering pulses can be adjusted in the −1 + 10 ps range.

Concerning the detection scheme, and also in light of our recent experience with the aforementioned EUV stimulated TG experiment, we foresee the use of both a cooled CCD camera in vacuum and fast photodiodes in combination with a boxcar amplifier. The latter can provide faster acquisition times, while the former can be used, in combination with a special setup, to map out the time dependence of the FWM signal into the spatial coordinate; using chirped pulses the frequency content of the FWM signal can also be mapped out on the CCD. Furthermore, the CCD detector will permit the full footprint of the FWM signal to be determined, which can be of relevance when the phase matching conditions are relaxed due to thin grating effects. The latter are very likely if one uses optical radiation for probing the FEL-induced EUV/soft X-ray gratings, since in those cases the penetration depth of the FEL radiation is usually shorter than the optical wavelength in the material. TG signals (either optical or EUV/soft X-ray) could be in principle detected both in transmission and in reflection geometry.

We finally mention the possibility to use continuous-wave optical probing with sub-nanosecond sampling to study dynamics longer than the nanosecond range and to use permanent gratings, created *in situ* by high-flux irradiation with FEL pulses, to generate local fields for HD-TG measurements.

5. Overview of initial EIS-TIMEX results

5.1. FEL-pump/laser-probe measurements

Preliminary pump–probe experiments based on an optical probe (at 780 nm wavelength with a pulse length of about 130 fs) and a FEL pump (at 42.3 nm wavelength with a pulse length of about 80 fs) have been carried out on a Si_3N_4 sample, deposited onto a Si substrate. This class of measurements was aimed at revealing a transient ultrafast change in the optical reflectivity of the sample as an effect of the electron transfer from the top valence to the bottom conduction band and the subsequent activation of intra-band absorption channels for 780 nm photons (Durbin *et al.*, 2012). Experiments show (Fig. 9) a sudden (∼200 fs) decrease of reflectivity at 780 nm of about 10% followed by a slower recovery of the original level associated with a gradual relaxation of hot electrons in the valence band.

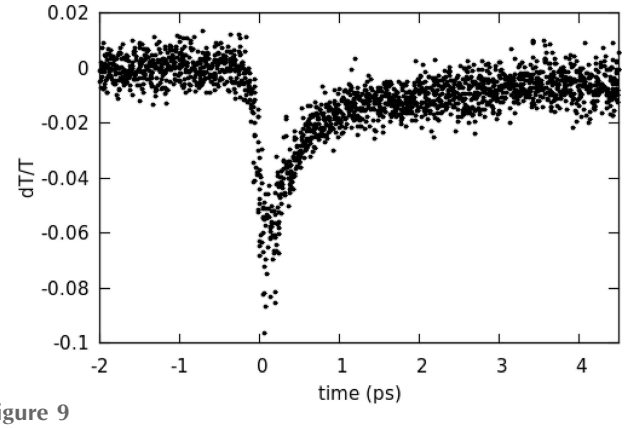

Figure 9
Transient variation of Si_3N_4 reflectivity at 780 nm driven by FEL excitation (pulse duration <100 fs).

The steep reflectivity drop, being an indication of the occurred longitudinal superposition between the pump and probe pulses, can be used as a marker for the 'time-zero' of the investigated dynamics. Such kind of measurement has been recently used to quantify the time-jitter affecting combined FEL/optical pump–probe measurements at EIS-TIMEX to less than 6 fs RMS, which qualifies as an unbeaten performance (Danailov *et al.*, 2014). The excellent pump–probe synchronization can be indeed appreciated from the accuracy of the data in Fig. 9, which were not subject to any post-processing treatment.

A vast variety of responses have been collected as a function of the pump wavelength, of the probe polarization, of the sample thickness and type of substrate in both reflection and transmission geometries, which lead us to recognize the role of interference effects that are due to the different penetration depths of the EUV FEL and infrared laser pulses (Casolari *et al.*, 2014).

5.2. Ultrafast reflectivity and absorption spectroscopy measurements

EIS-TIMEX intends to heavily exploit the tunability of the FEL source (Allaria *et al.*, 2012*b*) for spectroscopic purposes. Both reflectivity and absorption spectroscopies have been attempted so far on solid samples. Reflectivity measurements were carried out for example on a Ti sample deposited onto a Si substrate (roughness about 1 nm RMS) as a function of both FEL fluence and photon energy, the latter chosen just above the plasmon resonance (17.7 eV). A clear increase in

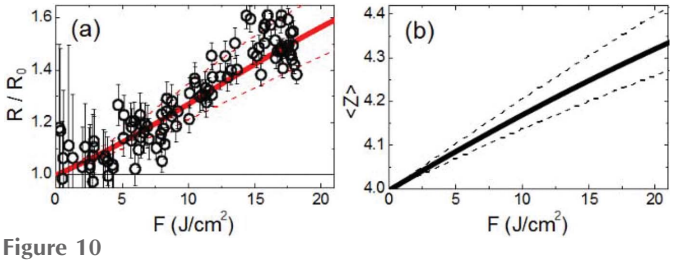

Figure 10
Fluence dependence of the relative reflectivity R/R_0 of Ti for $\omega = 18.9$ eV. The full red line comes from the Drude model developed to interpret the data (Bencivenga *et al.*, 2014*b*). From the same model the fluence trend of the mean ionization state $\langle Z \rangle$, shown as a full black line in panel (*b*), was derived; dashed lines in panel (*b*) indicate the confidence intervals.

the reflectivity at 18.9 eV was noticed for increasing FEL fluences, as shown in panel (*a*) of Fig. 10. We have shown (Bencivenga *et al.*, 2014*b*) that such reflectivity increase occurs also at 19.7 eV and 20 eV and that this effect can be reconducted, within a Drude model, to an increase of the plasma frequency, in turn due to ionization processes that lead to an ultrafast increase of the average free electron density within the time duration (<100 fs) of the FEL pulses, as depicted in panel (*b*) of Fig. 10.

Ultrafast absorption spectra at low fluence have been collected for several specimens [Al (Di Cicco *et al.*, 2014), Mg (Mincigrucci, 2015), Ge (Giangrisostomi, 2015)] and compared with similar data recorded at a synchrotron, providing a demonstration of the capabilities of FERMI to be tuned through a broad spectral range thanks to the seed laser radiation provided by an optical parametric amplifier. As an example, the absorption spectrum of a Ti foil (nominal thickness: 50 nm) is shown in Fig. 11.

Absorption spectra were then collected under high fluence conditions. In a first approach, an identical FEL pulse both probes and pumps the specimen, thus measuring the absorption of an excited sample. With a pulse duration shorter than 100 fs, the excitation is expected to be restricted to the electronic subsystem. Measurements of this kind are always

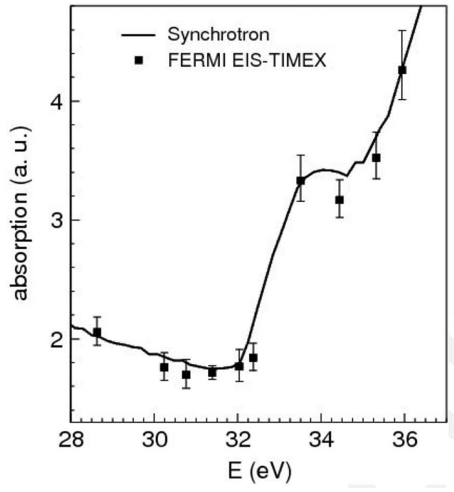

Figure 11
Absorption spectrum of Ti ($M_{2,3}$-edge) measured with both synchrotron (BEAR beamline, ELETTRA) and FEL (EIS-TIMEX beamline, FERMI) light.

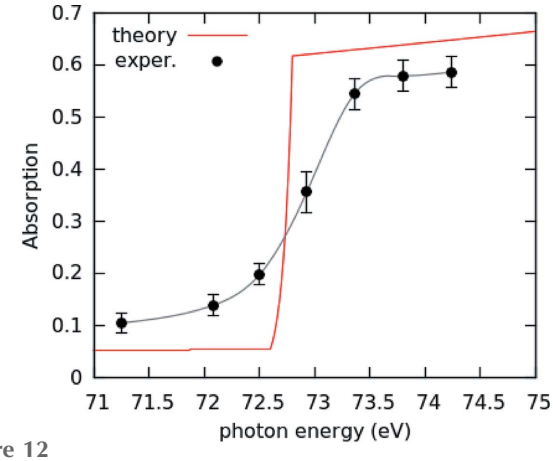

Figure 12
Absorption spectrum of Al at the $L_{2,3}$-edge collected at EIS-TIMEX at a fluence of about 0.2 J cm^{-2}, compared with the reference curve for a cold Al sample of thickness 35 nm (red curve, from the CXRO database). The gray curve is a guide to the eye.

conducted in a single-shot fashion, as the sample is damaged upon deposition of the pulse energy.

In Fig. 12, the $L_{2,3}$ absorption edge of an Al sample exposed to 60 fs FEL pulses at a fluence of about 0.2 J cm^{-2} is shown and compared with the theoretical absorption at normal conditions. The edge smearing reflects the rearrangement of the electronic population across the Fermi level as an effect of the ultrafast increase of the electron temperature and subsequent sub-100 fs thermalization. The shape of the absorption spectrum is compatible with a Fermi-like electron distribution corresponding to an electron temperature of about 0.5 eV.

When associated with a laser pump, the spectroscopic capabilities of the FERMI FEL probe can make accessible time-resolved absorption spectroscopy, thus providing sensitivity to the ultrafast dynamics of the excited electronic structure in a time scale from a few tens of femtoseconds up to about 10 ps. Preliminary pump–probe absorption experiments across the $L_{2,3}$-edge of Si (around 100 eV) indicated that the electronic structure of Si drastically changes on a time scale shorter than 1 ps when exposed to 130 fs laser pulses (at 390 nm). The relative variation of transmittance (Fig. 13) measured just below (99.58 eV) and above (100.8 eV) the edge can reflect, as discussed above for Al, both the rearrangement of the electron population across the Fermi level and the collapse of the band gap associated with a semiconductor-to-metal transition in Si (Johnson *et al.*, 2003).

5.3. FEL-pump/FEL-probe measurements

Very recently, time-resolved absorption measurements have been carried out on Si through the grazing-incidence delay-line positioned along the beam transport of FERMI. In this experiment the primary beam consisted of a double color emission (12.3 nm and 50 nm) and was split into two parts by the delay-line. A Parylene filter was used to block the long-wavelength radiation in the branch that should act as a probe, whereas an Al filter was used in the pump branch to remove the fraction of radiation at the shorter wavelength. The two pulses were superposed on the sample (with a thickness of

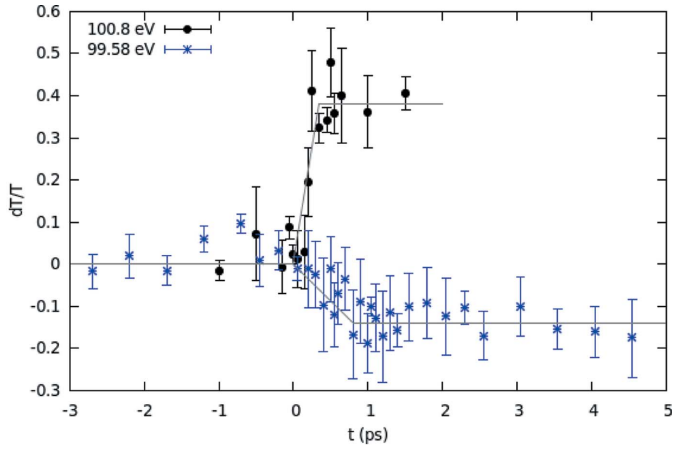

Figure 13
Relative variation of the transmission of a Si foil (thickness 100 nm) induced by an intense laser pump (pulse energy 25 µJ, wavelength 390 nm, length 130 fs), for different FEL probe wavelengths before (99.6 eV) and after (100.8 eV) the $L_{2,3}$-edge (pulse length <100 fs). Solid gray lines are guides to the eye.

150 nm, close to the attenuation length for the pump photons in Si) and the transmitted intensity was measured by a photodiode insensitive to the pump radiation. With this unique jitter-free FEL-pump/FEL-probe setup, the absorption measurements shown in Fig. 14 were collected. One can observe a very steep transmissivity jump, compatible with a FEL-induced ultrafast change in the electronic structure of the Si sample across the Fermi level that persists after the FEL pulse. Such a change, very similar to that observed with a 780 nm pump, suggests that the transmission variation is a temperature-driven irreversible process not dependent on the wavelength such as the metalization of the semiconductor. If this is the case, the metalization is demonstrated to occur in about 300 fs.

6. Conclusions and outlook

We reported on the present and forthcoming research activities at the basis of the EIS project, that is aimed at studying both the ultrafast evolution of condensed matter towards extreme thermodynamic conditions and the coherent nonlinear response of 'conventional' (*i.e.* not highly photoexcited) matter at EUV/soft X-ray wavelengths over a wide time scale range. The latter task will be pursued by the EIS-TIMER beamline (presently under construction), which is mainly focused on FWM experiments based on the TG approach and whose rationale is also based on the experience we made at our laser laboratory (Cucini *et al.*, 2011*a*,*b*, 2014), as well as on a proof-of-principle EUV-TG experiment we recently carried out (Bencivenga *et al.*, 2015) at another end-station using a simplified setup mixing EUV and visible radiation.

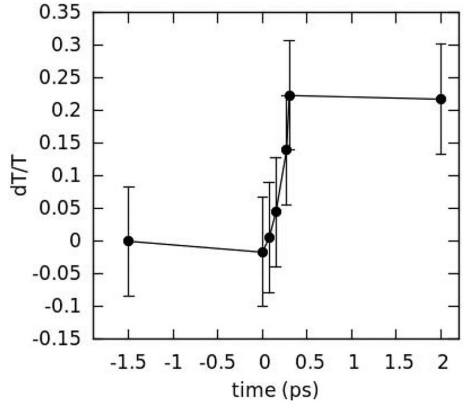

Figure 14
Time-resolved relative variation of transmission of a Si sample foil (thickness 150 nm) at 100.8 eV driven by absorption of intense FEL pulses (intensity ∼1 µJ, photon energy 24.8 eV, length <100 fs).

The study of matter under extreme conditions is being pursued at EIS-TIMEX, an instrument that is presently operational and available for users. We hereby reported on the results of the first experiments carried out in the last two years at EIS-TIMEX, in parallel with the instrumental commissioning program. These include ultrafast EUV reflectivity and transmissivity measurements (without explicit time resolution) on simple metals, which provided relevant information on the basic excitation mechanisms. Furthermore, ultrafast pump–probe experiments involving both FEL and optical pulses, as well as FEL-pump/FEL-probe experiments, have been carried out.

In the near future the EIS-TIMER end-station will start the commissioning program, while the pump–probe capabilities of both instruments will be substantially extended, also by exploiting the options for multi-color FEL emission of FERMI.

Acknowledgements

CM acknowledges support from the European Research Council through the grant N.202804-TIMER. COST Action MP1306 EUSpec is also acknowledged.

References

Adams, B. (2011). *Nat. Phys.* **7**, 675–676.
Allaria, E. *et al.* (2012*a*). *Nat. Photon.* **6**, 699–704.
Allaria, E. *et al.* (2012*b*). *New J. Phys.* **14**, 113009.
Allaria, E. *et al.* (2013). *Nat. Commun.* **4**, 2476.
Allaria, E., Callegari, C., Cocco, D., Fawley, W. M., Kiskinova, M., Masciovecchio, C. & Parmigiani, F. (2010). *New J. Phys.* **12**, 075002.
Battistoni, A., Bencivenga, F., Fioretto, D. & Masciovecchio, C. (2014). *Opt. Lett.* **39**, 5858–5861.
Bencivenga, F., Baroni, S., Carbone, C., Chergui, M., Danailov, M. B., De Ninno, G., Kiskinova, M., Raimondi, L., Svetina, C. & Masciovecchio, C. (2013). *New J. Phys.* **15**, 123023.
Bencivenga, F., Battistoni, A., Fioretto, D., Gessini, A., Sandercock, J. & Masciovecchio, C. (2012). *Rev. Sci. Instrum.* **83**, 103102.
Bencivenga, F., Capotondi, F., Casolari, F., Dallari, F., Danailov, M. B., De Ninno, G., Fausti, D., Kiskinova, M., Manfredda, M., Masciovecchio, C. & Pedersoli, E. (2014*a*). *Faraday Discuss.* **171**, 487.
Bencivenga, F., Cucini, R., Capotondi, F., Battistoni, A., Mincigrucci, R., Giangrisostomi, E., Gessini, A., Manfredda, M., Nikolov, I. P., Pedersoli, E., Principi, E., Svetina, C., Parisse, P., Casolari, F., Danailov, M. B., Kiskinova, M. & Masciovecchio, C. (2015). *Nature (London)*. In the press.

Bencivenga, F. & Masciovecchio, C. (2009). *Nucl. Instrum. Methods Phys. Res. A*, **606**, 785–789.

Bencivenga, F., Principi, E., Giangrisostomi, E., Cucini, R., Battistoni, A., D' Amico, F., Di Cicco, A., Di Fonzo, S., Filipponi, A., Gessini, A., Gunnella, R., Marsi, M., Properzi, L., Saito, M. & Masciovecchio, C. (2014*b*). *Sci. Rep.* **4**, 4952.

Borghes, R., Chenda, V., Curri, A., Kourousias, G., Lonza, M., Prica, M., Pugliese, R. & Passos, G. (2013). *14th International Conference on Accelerator and Large Experimental Physics Control Systems*, Vol. 1, p. 1481.

Boyd, R. W. (2010). *Nonlinear Optics*, 3rd ed. New York: Academic Press.

Burkel, E. (2000). *Rep. Prog. Phys.* **63**, 171–232.

Casolari, F., Bencivenga, F., Capotondi, F., Giangrisostomi, E., Manfredda, M., Mincigrucci, R., Pedersoli, E., Principi, E., Masciovecchio, C. & Kiskinova, M. (2014). *Appl. Phys. Lett.* **104**, 191104.

Cinquegrana, P., Cleva, S., Demidovich, A., Gaio, G., Ivanov, R., Kurdi, G., Nikolov, I., Sigalotti, P. & Danailov, M. B. (2014). *Phys. Rev. ST Accel. Beams*, **17**, 040702.

Corso, A., Zuppella, P., Windt, D., Zangrando, M. & Pelizzo, M. (2012). *Opt. Express*, **20**, 8006.

Cucini, R., Battistoni, A., Gessini, A., Bencivenga, F., Principi, E., Saito, M., D'Amico, F., Sergo, R. & Masciovecchio, C. (2014). *Opt. Lett.* **39**, 5110–5113.

Cucini, R., Bencivenga, F. & Masciovecchio, C. (2011*b*). *Opt. Lett.* **36**, 1032–1034.

Cucini, R., Bencivenga, F., Zangrando, M. & Masciovecchio, C. (2011*a*). *Nucl. Instrum. Methods Phys. Res. A*, **635**, S69–S74.

Cundiff, S. T. & Mukamel, S. (2013). *Phys. Today*, **66**, 44.

Danailov, M. B., Bencivenga, F., Capotondi, F., Casolari, F., Cinquegrana, P., Demidovich, A., Giangrisostomi, E., Kiskinova, M. P., Kurdi, G., Manfredda, M., Masciovecchio, C., Mincigrucci, R., Nikolov, I. P., Pedersoli, E., Principi, E. & Sigalotti, P. (2014). *Opt. Express*, **22**, 12869–12879.

Dhar, L., Rogers, J. A. & Nelson, K. A. (1994). *Chem. Rev.* **94**, 157–193.

Di Cicco, A., Bencivenga, F., Battistoni, A., Cocco, D., Cucini, R., D'Amico, F., Di Fonzo, S., Filipponi, A., Gessini, A., Giangrisostomi, E., Gunnella, R., Masciovecchio, C., Principi, E. & Svetina, C. (2011*a*). *Proc. SPIE*, **8077**, 807704.

Di Cicco, A., D'Amico, F., Zgrablic, G., Principi, E., Gunnella, R., Bencivenga, F., Svetina, C., Masciovecchio, C., Parmigiani, F. & Filipponi, A. (2011*b*). *J. Non-Cryst. Solids*, **357**, 2641–2647.

Di Cicco, A., Hatada, K., Giangrisostomi, E., Gunnella, R., Bencivenga, F., Principi, E., Masciovecchio, C. & Filipponi, A. (2014). *Phys. Rev. B*, **90**, 220303.

Durbin, S., Clevenger, T., Graber, T. & Henning, R. (2012). *Nat. Photon.* **6**, 111–114.

Emma, P. *et al.* (2010). *Nat. Photon.* **4**, 641–647.

Frassetto, F., Miotti, P., Callegari, C., de Simone, M., Finetti, P., Giangrisostomi, E., Grazioli, C., Iesari, F., Kivimaki, A., Mincigrucci, R., Principi, E., Stagira, S., Di Cicco, A., Coreno, M. & Poletto, L. (2014). *Proc. SPIE*, **9210**, 92100E.

Gallmann, L., Cirelli, C. & Keller, U. (2012). *Annu. Rev. Phys. Chem.* **63**, 447–469.

Giangrisostomi, E. (2015). In preparation.

Glover, T., Fritz, D., Cammarata, M., Allison, T., Coh, S., Feldkamp, J., Lemke, H., Zhu, D., Feng, Y., Coffee, R., Fuchs, M., Ghimire, S., Chen, J., Shwartz, S., Reis, D., Harris, S. & Hastings, J. (2012). *Nature (London)*, **488**, 603–608.

Goulielmakis, E., Schultze, M., Hofstetter, M., Yakovlev, V. S., Gagnon, J., Uiberacker, M., Aquila, A. L., Gullikson, E. M., Attwood, D. T., Kienberger, R., Krausz, F. & Kleineberg, U. (2008). *Science*, **320**, 1614–1617.

Guehr, M., Penn, G. & Zholents, A. A. (2014). *Phys. Rev. Lett.* **113**, 024801.

Hara, T., Inubushi, Y., Katayama, T., Sato, T., Tanaka, H., Tanaka, T., Togashi, T., Togawa, K., Tono, K., Yabashi, M. & Ishikawa, T. (2013). *Nat. Commun.* **4**, 2919.

Itatani, J., Levesque, J., Zeidler, D., Niikura, H., Pépin, H., Kieffer, J. C., Corkum, P. B. & Villeneuve, D. M. (2004). *Nature (London)*, **432**, 867–871.

Johnson, S. L., Heimann, P. A., Lindenberg, A. M., Jeschke, H. O., Garcia, M. E., Chang, Z., Lee, R. W., Rehr, J. J. & Falcone, R. W. (2003). *Phys. Rev. Lett.* **91**, 157403.

Lee, R. W., Moon, S. J., Chung, H.-K., Rozmus, W., Baldis, H. A., Gregori, G., Cauble, R. C., Landen, O. L., Wark, J. S., Ng, A., Rose, S. J., Lewis, C. L., Riley, D., Gauthier, J.-C. & Audebert, P. (2003). *J. Opt. Soc. Am. B*, **20**, 770–778.

Li, M., Menon, S., Nibarger, J. P. & Gibson, G. N. (1999). *Phys. Rev. Lett.* **82**, 2394–2397.

Lovesey, S. W. (1986). *Theory of Neutron Scattering from Condensed Matter, International Series of Monographs on Physics*, Vol. 72. Clarendon Press.

Lutman, A. A., Coffee, R., Ding, Y., Huang, Z., Krzywinski, J., Maxwell, T., Messerschmidt, M. & Nuhn, H. (2013). *Phys. Rev. Lett.* **110**, 134801.

Masciovecchio, C., Cocco, D. & Gessini, A. (2004). *AIP Conf. Ser.* **705** 1190–1196.

Maznev, A. A., Nelson, K. A. & Rogers, J. (1998). *Opt. Lett.* **23**, 1319–1321.

Mincigrucci, R. (2015). In preparation.

Morgner, U. (2010). *Nat. Photon.* **4**, 14–15.

Mukamel, S. (1995). *Principles of Nonlinear Optical Spectroscopy*. Oxford University Press.

Patterson, B. (2010). *Resource Letter on Stimulated Inelastic X-ray Scattering at an XFEL*. Report SLAC-TN-10-026. SLAC, Stanford, CA, USA.

Principi, E., Cucini, R., Filipponi, A., Gessini, A., Bencivenga, F., D'Amico, F., Di Cicco, A. & Masciovecchio, C. (2012). *Phys. Rev. Lett.* **109**, 025005

Shwartz, S., Fuchs, M., Hastings, J., Inubushi, Y., Ishikawa, T., Katayama, T., Reis, D., Sato, T., Tono, K., Yabashi, M., Yudovich, S. & Harris, S. (2014). *Phys. Rev. Lett.* **112**, 163901.

Svetina, C., Cocco, D., Di Cicco, A., Fava, C., Gerusina, S., Gobessi, R., Mahne, N., Masciovecchio, C., Principi, E., Raimondi, L., Rumiz, L., Sergo, R., Sostero, G., Spiga, D. & Zangrando, M. (2012). *Proc. SPIE*, **8503**, 850302.

Svetina, C., Sostero, G., Sergo, R., Borghes, R., Callegari, C., D'Amico, F., Bencivenga, F., Masciovecchio, C., Di Cicco, A. & Cocco, D. (2011). *Nucl. Instrum. Methods Phys. Res. A*, **635**(Suppl. 1), S12–S15.

Tamasaku, K., Sawada, K., Nishibori, E. & Ishikawa, T. (2011). *Nat. Phys.* **7**, 705–708.

Tanaka, S. & Mukamel, S. (2002). *Phys. Rev. Lett.* **89**, 043001.

Wynne, K., Galli, C. & Hochstrasser, R. (1994). *J. Chem. Phys.* **100**, 4797–4810.

Zangrando, M., Abrami, A., Bacescu, D., Cudin, I., Fava, C., Frassetto, F., Galimberti, A., Godnig, R., Giuressi, D., Poletto, L., Rumiz, L., Sergo, R., Svetina, C. & Cocco, D. (2009). *Rev. Sci. Instrum.* **80**, 113110.